Influence of ZIF-67 Drying Temperatures on the Structure and Properties of PEBAX® MH-1657/ZIF-67 Mixed Matrix Membranes for Enhanced CO_2/N_2 Separation

Paula S. Pacheco[a]* , *Sônia Faria Zawadzki[b]* , *Daniel Eiras[a]*

[a]*Universidade Federal do Paraná (UFPR), Programa de Pós-Graduação em Ciência e Engenharia de Materiais, Curitiba, PR, Brasil.*

[b]*Universidade Federal do Paraná (UFPR), Programa de Pós-Graduação em Química, Curitiba, PR, Brasil.*

This study synthesized mixed matrix membranes (MMMs) using PEBAX® MH-1657 and ZIF-67 with varying particle concentrations (1, 3, and 5 wt%) to assess permeability and selectivity. ZIF-67 nanoparticles were prepared using the solvothermal method with methanol and characterized. Permeation tests were conducted at 10 and 15 bar using N_2 and CO_2. The analysis revealed ZIF-67 particles with an approximate diameter of 280 nm and confirmed characteristic sodalite peaks. The ideal CO_2/N_2 selectivity reached 67 (CO_2 permeability = 132 ± 3.5 Barrer) at 15 bar. The impact of ZIF-67 varied with pressure and composition; at 10 bar, CO_2/N_2 selectivity decreased compared to pure PEBAX®; however, at 15 bar, the 1 wt% ZIF-67 membrane exhibited superior selectivity, surpassing Robeson's upper bound. The results indicate that ZIF-67 enhances the permeability and selectivity of PEBAX®, with superior performance observed at lower concentrations.

Keywords: *Mixed matrix membranes, gas separation, ZIF-67 and PEBAX® MH-1657.*

1. Introduction

Gas separation using polymer membranes is considered a simple process with low energy consumption compared to other existing technologies like distillation and absorption. Furthermore, it can be considered an environmentally friendly process as gas separations using membranes occur based on a chemical potential difference between the membrane sides, which acts as a driving force for mass transport. However, its application is still limited by low productivity and thermal stability[1-3]. The purification of natural gas is a significant example of the application of membrane separation processes. Natural gas is predominantly composed of methane (CH_4), which accounts for 70% to 90% of its composition. However, the presence of other impurity gases, such as carbon dioxide (CO_2), requires a purification step to increase the heat value and prevent corrosion of pipelines[4-6]. Although there are currently available separation processes, such as amine absorption, for this purpose, the use of these processes poses several operation and environment challenges that can be overcome by membrane separation processes. Nevertheless, further improvements are needed for membrane separation processes to be able to replace conventional separations in all industrial-scale applications. Natural gas treatment processes typically occur at relatively high pressures, ranging from 30 to 60 bars. Additionally, natural gas streams contain a variety of components, some of which (such as water, carbon dioxide, and C_4+ hydrocarbons) can cause membrane degradation and plasticization. In addition to these components, the gas flow may contain entrained oil mist, fine particles, and hydrocarbon vapors, which can easily accumulate on the membrane surface[7-10].

The predominant constraint within membrane separation processes lies in the endeavor to attain elevated purity levels at substantial throughput rates. This predicament arises from the intricate balance between membrane permeability and selectivity. Augmenting membrane permeability diminishes the requisite surface area for processing a given volume of gas, thereby mitigating capital expenditures. However, heightened membrane selectivity becomes imperative for the attainment of superior gas product purity. This delicate equilibrium represents an empirical threshold grounded in experimental data, constituting a pivotal hurdle in the realm of membrane science[8,9,11,12]. Within conventional polymer membranes, a well-documented trade-off exists between selectivity and permeability, wherein elevated selectivity often coincides with diminished permeability. This trade-off in separation membranes is widely acknowledged and was mathematically elucidated by Robeson in 1991, with subsequent revisitations in 2008. Generally, polymers with higher permeability tend to exhibit lower selectivity, and vice versa[9,12,13].

The chemical structure of the polymer used in membrane fabrication plays a crucial role in determining its permeability and selectivity. Additionally, structural characteristics such as thickness, density, and porosity also have a significant impact on these properties[13-16]. In gas permeation processes involving membranes, the transport of gas molecules is governed by permeability (P). Permeability is defined as the product of the diffusion coefficient (D) and the solubility coefficient (S), as represented by Equation 1. This equation characterizes the diffusive flux (J) of the permeating molecule across a polymeric membrane with a specific thickness (l), influenced by the pressure gradient across the membrane

*e-mail: paula.sacchelli@gmail.com

(ΔP). The ideal selectivity (αA/B) characterizes a membrane's effectiveness in separating a gas mixture comprising gases A and B. It is quantifiable using Equation 2, where P_A denotes the permeability of the more permeable gas in the gas pair under consideration, divided by the permeability of the less permeable gas (P_B)[14,17]. The kinetic diameter and shape of gas molecules emerge as pivotal parameters influencing the diffusion coefficient due to the constrained mobility of polymer chains[18]. The membrane's ability to impede penetrants with minor steric differences significantly shapes membrane selectivity, thereby directly influencing the outcome of the gas separation process. Gas molecules exhibiting solubility parameters similar to those of the membrane polymer are more likely to manifest higher permeation rates[18-21].

$$\frac{Jl}{\Delta p} = P = D\,S \qquad (1)$$

$$\alpha_{A/B} = \frac{P_A}{P_B} \qquad (2)$$

Because the relationship between selectivity and permeability is a common challenge in all polymeric membranes, researchers are constantly searching for new materials and developing structures with improved chemical and thermal stability, high permeability, and high selectivity compared to conventional polymeric membranes[21-23]. A promising approach to improve these characteristics is the use of copolymers, which allow the combination of desirable properties through the selection of suitable polymers[15,22,23]. Copolymers are materials composed of one or more monomers with different chemical structures, which confer the desired properties. An example is the formation of a copolymer that combines rigid groups and more flexible groups, resulting in a material with a favorable combination of properties, depending on the specific application[22,24-27].

One notable example is PEBAX® MH-1657, a commercially available copolymer of great interest in the field of polymeric membranes. Its composition consists of 60% by weight of poly(ethylene oxide) (PEO) and 40% of polyamide-6 (PA). The presence of polyamide in the polymer chain provides mechanical strength to the material, while the poly(ethylene oxide) (PEO) segment imparts higher permeability to CO_2[6,23,28-30]. PEBAX® exhibits superior selectivity for CO_2 compared to light gases such as N_2 and CH_4. This selectivity is attributed to the higher affinity of the PEO segment of PEBAX® with CO_2 due to the presence of polar groups, in contrast to N_2 and CH_4, which are nonpolar gases. However, the presence of PEO segments would not be sufficient to provide the necessary mechanical strength for membrane application[30,31]. Therefore, it is necessary to combine this segment with a more rigid polymer block, such as polyamide (PA). The presence of polyamide gives PEBAX® high mechanical strength, which is related to the crystallinity present in the PA fraction. Although PEBAX® exhibits great flexibility and processability, its gas separation performance is limited by the trade-off between permeability and selectivity[32-34].

A promising strategy to improve the selectivity-permeability relationship in polymeric membranes is the use of mixed matrix membranes composed of PEBAX® and zeolitic imidazolate frameworks (ZIF) like ZIF-67[34-37]. These membranes have the potential to outperform conventional polymeric membranes in terms of selectivity and permeability. The combination of the sieving properties of metal-organic frameworks (MOFs) with the film-forming capability of the polymer matrix allows the production of mixed matrix membranes for different application requirements[38,39]. These membranes are obtained by mixing polymers to form the continuous phase (Phase A) and adding molecular sieves such as zeolites, carbon molecular sieves, and their derivatives to form the dispersed phase (Phase B). This arrangement enables the separation of gases based on the size and geometry of the gas molecules[36,38,40].

Excellent candidates for the separation of small kinetic diameter gas molecules such as CO_2, N_2, and CH_4 are ZIFs. The imidazolate ligands present in the structures of ZIFs confer them with higher hydrophobicity compared to other fillers, promoting good interfacial compatibility with polymers[25,31,41,42]. A notable example is ZIF-67, formed by linking 2-methylimidazolate anions and cobalt cations, with a pore size of approximately 0.34 nm. This dimension is intermediate to the kinetic diameters of CO_2 (0.33 nm) and larger gases such as N_2 (3.64 nm) and CH_4 (0.38 nm). Thanks to its suitable pore size and selective CO_2 adsorption ability, ZIF-67 exhibits excellent performance as a molecular sieve in separating CO_2/N_2 and CO_2/CH_4 gas pairs, with kinetic diameters of 0.33/0.36 nm and 0.33/0.38 nm, respectively[39,43,44].

Mixed matrix membranes have been considered as promising candidates for gas separation because they combine the processability and mechanical properties of polymer membranes with the selectivity and permeability of zeolites. Nevertheless, the production of mixed matrix membranes has proved to be a challenge due to the incompatibility between the polymer matrix and the inorganic zeolites[31,35,45]. The application of zeolitic imidazolate frameworks promises to reduce or eliminate the interface problems observed in conventional mixed matrix membranes which has encouraged several publications in the area. Moreover, a lot of effort has been devoted to the incorporation of ZIFs in glassy polymers, but there were not many publications on mixed matrix membranes produced with rubbery polymers or copolymers until PEBAX® has been discovered as a promising candidate for gas separation. Among these publications, there is no information on the effect of upstream pressure on properties of ZIF-based mixed matrix membranes[36,39,43,45].

Mixed matrix membranes composed solely of PEBAX® MH-1657 and ZIF-67 have been the subject of few studies in the literature. Other investigations have reported the use of PEBAX® MH-1657 MMMs with other fillers, such as Zeolites (4A) and ZIF-8, or the addition of other polymers alongside PEBAX® in the continuous matrix phase[44-49]. Meshkat et al.[36] produced PEBAX® MH-1657 /ZIF-67 membranes to evaluate the incorporation of ZIF-67 in polymeric matrices for gas separation properties. The study investigated the performance of MMMs composed of PEBAX® MH-1657 / ZIF-67 and PEBAX® MH-1657 /ZIF-8 in the separation of gases, including CO_2 from N_2 and CH_4. The addition of ZIF-67 and ZIF-8 led to a 130% and 85% increase in CO_2 permeability compared to pure PEBAX® MH-1657.

Influence of ZIF-67 Drying Temperatures on the Structure and Properties of PEBAX® MH-1657/ZIF-67 Mixed
Matrix Membranes for Enhanced CO_2/N_2 Separation

3

ZIF-67 outperformed ZIF-8 in terms of ideal selectivity for CO_2/N_2 and CO_2/CH_4 gas pairs, attributed to its role in facilitating CO_2 diffusion and ZIF-8's enhancement of CO_2 solubility due to strong electrostatic interactions between the Zn metal center of ZIF-8 and CO_2 molecules[36]. Zhao et al.[50] fabricated MMMs of PEBAX® MH-1657, ZIF-67, and ZIF-67-L for CO_2/N_2 separation. Optimal performance was achieved with PEBAX® MH-1657 /ZIF-67-L MMMs with a 10% by weight loading, surpassing pure PEBAX® MH-1657. It exhibited a 74.1% improvement in CO_2 permeability and a 23.6% improvement in CO_2/N_2 selectivity. Tien et al.[48] developed defect-free microporous ZIF-8 and ZIF-67 membranes on alumina supports using the secondary growth technique for propylene separation from propylene/propane gas mixtures. ZIF-8 outperformed ZIF-67 with a separation factor of 76 compared to 5 for ZIF-67. Although ZIF-67 did not achieve the expected selectivity, it exhibited higher permeability than ZIF-8. The significant improvement in ZIF-8's selectivity was attributed to structural "gate-opening" alterations, which widened the membrane pores and allowed propylene to permeate while retaining larger propane molecules.

One of the main challenges in producing MOF-based MMMs using green solvents is the instability of MOFs in an aqueous environment. Most MOF structures are unstable in aqueous solutions and cannot be used in the preparation of PEBAX® membranes due to their weak hydrothermal stability. The instability of ZIF-67 in water can be attributed to the specific presence of methylimidazole and Co^{2+} ions[27,36,46,47,50]. Furthermore, the hydrophobic surfaces hinder the homogeneous dispersion of the fillers in water, making the fabrication of these membranes even more challenging. Previous studies have shown the degradation of ZIF-8 in aqueous media, both in dynamic stability tests and static durability tests in pure water. The hydrolysis of ZIF-8 under ambient conditions in aqueous media has been identified as the cause of this instability[26,43,51,52].

Recent studies have demonstrated that it is possible to improve the stability of MOFs in aqueous environments through changes in their morphology. For example, modifying the traditional tetrahedral morphology of ZIF-67 to preferential growth in a single direction, such as ZIF-67 nanosheets, has resulted in improved thermal stability in water. This is due to the less exposed Co-N bonds and lower surface energy of the crystal faces. Additionally, membranes containing lower concentrations of ZIF-67 nanosheets have shown enhanced performance compared to pure polymer membranes and unstable ZIF-67-based MMMs[27,43,46,52-54]. On the other hand, Meshkat et al.[36], produced MMM/ZIF-67 in methanol with particles of an average size of approximately 300 nm and did not observe significant chemical interactions between the polymer and ZIF-67 particles, except for a slight interaction between the metal lone pair and the amide nitrogen in PEBAX®.

Considering the importance of mixed matrix membranes to improve the scope of applications of membrane separation processes and the properties of ZIF-67, in this study, our focus lies on the characterization of synthesized ZIF-67 structures, achieved through solvothermal synthesis employing methanol as the solvent and cobalt nitrate as the metallic source. The investigation into the drying conditions

becomes imperative considering the substantial impact this variable imparts on various properties of the formed particles. In the process of MOF synthesis, with a specific emphasis on ZIFs, the drying stage plays a critical role in defining the final material characteristics. The predominant effects of the drying temperature encompass particle size, morphology, surface area, crystallinity, stability, and interconnection among particles. These variables, in turn, play a crucial role in the gas separation process[55,56]. An experimental approach at higher pressures, ranging from 10 to 15 bar, will provide a deeper understanding of the impact of feed pressure on PEBAX® MH-1657/ZIF-67 MMMs and how the presence of synthesized ZIF-67 influences the gas transport properties of these membranes. Therefore, this study is relevant for optimizing the synthesis and performance of MOFs in various applications, such as gas storage and purification, catalysis, and controlled drug release[55-58].

2. Materials and Methods

2.1. Materials

Polyether-b-amide copolymer PEBAX® MH-1657 from Arkema Brazil was used as matrix to produce the membranes. Ethanol PA (MW=46.07 g/mol, 98.5%) was used as co-solvent with distilled water. The materials used for the synthesis of ZIF-67 nanoparticles were 2-methylimidazole (MW=82.10 g/mol, 99%) from Sigma Aldrich, cobalt nitrate hexahydrate (MW=291.03 g/mol, 98%) and methanol (MW=32.04 g/mol, 98%) from Êxodo Científica. CO_2 2.8 (99,8%), N_2 industrial grade and CH_4 2.5 (99.5%) were used to test the permeability of the membranes.

2.2. Synthesis of ZIF 67 nanoparticles

The synthesis of ZIF-67 was adapted from Meshkat et al.[36]. Two solutions were prepared: (a) 2.872 g of cobalt nitrate hexahydrate $Co(NO_3)_2 \cdot 6H_2O$ was dissolved in 200 mL of methanol; (b) 6.488 g of 2-methylimidazole (2-MeIM) was dissolved in 200 mL of methanol. The molar ratio was 1:8:1000 $Co(NO_3)_2 \cdot 6H_2O$: 2-MeIM: Methanol). Then, solution (a) was quickly mixed into (b) under vigorous stirring for 1 min and left undisturbed overnight. The nanoparticles were separated by centrifugation using an Edutec digital centrifuge at 4.000 rpm for 30 minutes and washed with methanol three times. Finally, the resulting material was divided into 2 portions and dried in a Fanem model 515/2-C drying oven: (a) at 100 °C for 24 hours and (b) at 25 °C for 48 hours.

2.3. Membrane Preparation

2.3.1. PEBAX® Membranes

Neat PEBAX® MH-1657 membranes were prepared using a reflux system consisting of a flask and condenser under an inert N_2 atmosphere. The polymer was dissolved in a 70/30 ethanol-water solution at a concentration of 3 wt%. The dissolution process took place under constant stirring at a temperature of 90 °C for approximately 3 hours. Once the polymer was completely dissolved, the solution was poured into Teflon® petri dishes, covered with glass slides, and left

to dry at room temperature for 48 hours to allow for gradual solvent evaporation. After the drying period, the glass slides were removed, and the membranes were further dried in a vacuum oven at 50 °C for 24 hours to ensure the complete removal of any remaining solvent.

2.3.2. Mixed Matrix Membranes (MMMs)

PEBAX® MH-1657 /ZIF-67 mixed matrix membranes were prepared using a reflux system and constant stirring, following the procedure previously described. An ethanol-water solution with a ratio of 70/30 was divided, and two-thirds of this solution were employed for dissolving the PEBAX® at a concentration of 3 wt%. Concurrently, the different concentrations of nanoparticles (1%, 3%, and 5% wt% relative to the polymer weight) were dispersed in one-third of the final solvent quantity using an ultrasonic bath for 30 minutes. Subsequently, the ZIF-67 suspension particles were added to the PEBAX® solution and stirred for 24 hours under the same conditions. Once again, the resulting solution was poured into Teflon® petri dishes and left at room temperature for 48 hours. To ensure the thorough removal of solvents, the membranes were then dried in a vacuum oven at 50 °C for 24 hours. Table 1 presents the compositions and nomenclature adopted in this study for the MMM dried at different temperatures.

3. Analysis

The morphology of ZIF-67 nanoparticles was characterized by SEM using a JEOL JMS 6360-LV microscope with accelerating voltage of 15kV, magnification of 75kx, and resolution of 500nm. The membranes were cryofractured by immersion in liquid nitrogen for 1 hour. The nanoparticles were poured on a carbon tape and coated with a film of gold. Wide Angle X-Ray Diffraction (WAXD) was employed to evaluate the crystalline structure of PEBAX® and the influence of ZIF- 67 nanoparticles in the crystallization of PEBAX®. Fourier Transform Infrared Spectroscopy (FTIR) was performed using a Bruker FTIR 70v instrument with an attenuated total reflection (ATR) accessory. The Brunauer-Emmet-Teller surface area analysis (BET) was performed in a Quantachrome NovaWin equipment with N_2 at 73K. The samples were degassed overnight before analysis. Twenty points were analyzed between 0 and 1 (P/P_o). The analysis of the surface area was performed by the Data Acquisition and Reduction software from NOVA instruments.

Differential Scanning Calorimetry (DSC) was used to evaluate the glass transition temperature, the melt and crystallization behavior of PEBAX® and PEBAX® MH-1657/ ZIF-67 membranes. The tests were conducted in a NETZSCH DSC 200F3 calorimeter with two heating sequences. The samples were heated to 120°C to remove moisture, cooled to -70°C, and then heated to 250°C to remove thermal and processing history. Then the samples were cooled to -70°C and heated to 250°C. The heating rate was 10°C/min, and the nitrogen flux was 20 mL/min. The degree of crystallinity (%X_c) of PEBAX® MH-1657 was determined using fusion enthalpy and crystallization enthalpy, as defined in Equation 3. Equation 4 was then applied to calculate the total degree of crystallinity in the membranes (%X_t). ΔH_m represents the enthalpy associated with the melting peak (T_m), while ΔH_0 denotes the fusion enthalpy of the 100% crystalline phases, which are 230 J/g for PA and 166.4 J/g for PEO[16,40]. The variables ϕ represent the mass fractions of PEO and PA within PEBAX® MH-1657 (PEO=60%; PA=40%), and $\phi_{PEBAX® MH-1657}$ corresponds to the proportion of PEBAX® MH-1657 in the mixed matrix membranes, considering the percentage of added particles.

$$\%X_c = \left[\frac{\Delta H_m}{\phi * \Delta H_0} \right] *100 \qquad (3)$$

$$\%X_t = \frac{\left(\%X_{cPEO} * \phi_{PEO} + \%X_{cPA} * \phi_{PA} \right)}{\phi_{PEBAX1657}} \qquad (4)$$

3.1. Gas permeation tests

The permeability and ideal selectivity of N_2, CH_4 and CO_2 were determined using a variable volume/constant pressure permeation cell (Figure 1). The system consists of a stainless still cell that is connected to the feed gas on the upstream and a bubble soap flowmeter on the downstream. The gases were industrial grades, the test temperature was 35 °C and the upstream pressures were 10 and 15 bar for each gas. The separation area was 17.34 cm². For each membrane the flow rate on the
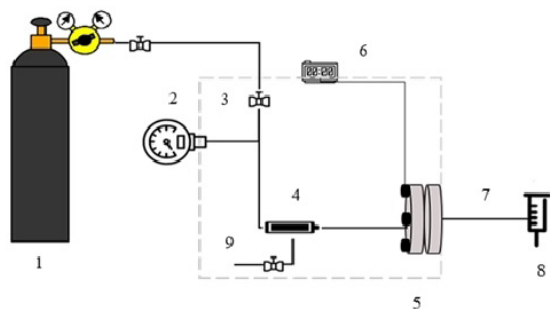

Figure 1. Schematic representation of the permeation cell used in this work. 1- Gas Cylinder; 2-Manometer; 3- Oven; 4- Gas reservoir; 5- Permeation cell; 6- Temperature Control; 7- Permeate; 8- Flowmeter; 9- Retentate.

Table 1. Compositions and nomenclature adopted for the PEBAX® MH-1657/ZIF-67 MMMs.

Sample	Composition of PEBAX 1657	Composition of ZIF-67	Drying temperature of ZIF-67
1% T.25 °C	3% PEBAX	1% ZIF-67	25 °C
3% T.25 °C	3% PEBAX	3% ZIF-67	25 °C
5% T.25 °C	3% PEBAX	5% ZIF-67	25 °C
1% T.100 °C	3% PEBAX	1% ZIF-67	100 °C
3% T.100 °C	3% PEBAX	3% ZIF-67	100 °C
5% T.100 °C	3% PEBAX	5% ZIF-67	100 °C

Influence of ZIF-67 Drying Temperatures on the Structure and Properties of PEBAX® MH-1657/ZIF-67 Mixed
Matrix Membranes for Enhanced CO_2/N_2 Separation

5

downstream was measured until the difference between two measurements was within 5%. Two membranes were tested for each sample unless the deviations between the duplicates were too high in which case more tests were conducted[12,19,30]. Gas permeability was calculated using Equation 5 and ideal selectivity was calculated using Equation 6.

$$P = \frac{\Delta V}{\Delta t}\left[\frac{cm^3}{s}\right]\frac{273[K]}{T[K]}\frac{t[cm]}{A[cm^2]\Delta P[cmHg]} \times 10^{10}[Barrer]. \quad (5)$$

$$\alpha_{A/B} = \frac{P_A}{P_B} \quad (6)$$

In which $\frac{\Delta V}{\Delta t}$ is the flow rate measured with the flowmeter, T is the test temperature, t is the membrane thickness, A is the
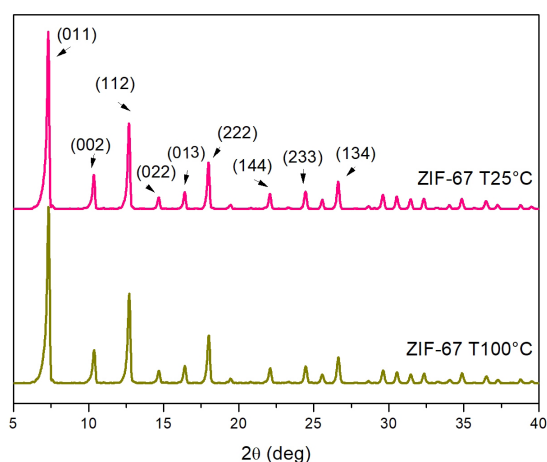

Figure 2. ZIF-67 nanoparticles curves.

permeation area, ΔP is the difference between upstream and downstream pressure, and P_A and P_B are the permeabilities of the most permeable and less permeable gases, respectively.

4. Discussion

4.1. Synthesis of ZIF-67 particles

WAXD characterization was performed to investigate the crystalline structure and phase purity of the synthesized ZIF-67 nanoparticles. The characteristic diffraction peaks revealed that the synthesized particles are consistent with reported ZIF-67 patterns, indicating successful particle synthesis. The XRD spectra shown in Figure 2 exhibit sharp and clean peaks characteristic of ZIF-67 at 7.3°, 10.3°, 12.6°, and 18.03°, corresponding to the (0 11), (002), (112), and (222) planes, respectively, for both cases presented. The similarity between the presented diffraction patterns was expected, as according to the theory of crystal nucleation and growth, the crystalline core of ZIF-67 is produced when cobalt ions react with MeIM at room temperature. The fact that the particles were dried at different temperatures does not alter the material's structure[43,45-48]. The respective values of the specific surface area (BET) for the ZIF-67 crystals showed a high surface area of 1,852 m^2/g for the structures dried at 25 °C and 1,678 m^2/g for the crystals dried at 100 °C. The higher surface area exhibited by the ZIF dried at 25°C can be justified by the presence of residual solvent from the synthesis within the structure, resulting in a larger pore volume[44,46-48,50].

Figure 3 shows the scanning electron microscopy (SEM) images of particles dried at 25°C (a) and 100°C (b), in both cases, a typical ZIF-67 structure is observed, with well-defined facets, edges, and corners. This morphology is consistent with the results reported in the literature. The presence of well-defined facets indicates high purity and homogeneity of
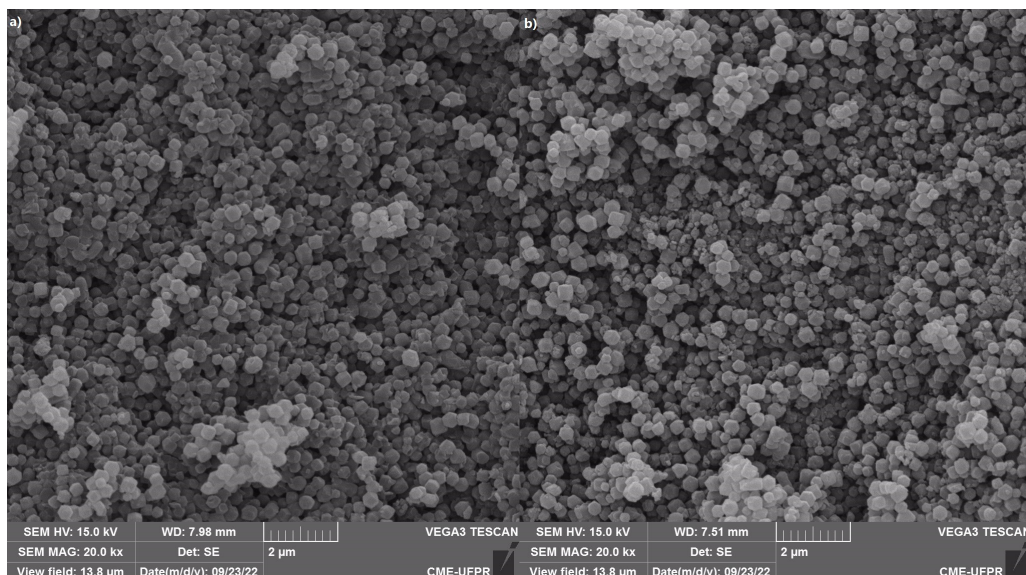

Figure 3. ZIF-67 particles synthesized and dried at different temperatures: (a) ZIF- 67 dried at 25°C (b) ZIF- 67 dried at 100 °C, both at 20 kx magnification.

the synthesized particles, while the sharp edges and corners suggest good crystallinity of the material[46,47]. However, it is also possible to notice the presence of ZIF-67 agglomerates for both drying conditions. The particle size and morphology are related to the reactivity of cobalt salt, molar ratios MeIM/Co^{2+}, and experimental conditions. The excess of imidazolic ligand relative to cobalt increases the nucleation rate of crystals. Consequently, as the molar proportion of the ligand increases, the particle size in the crystal decreases. The small crystals formed by nucleation are covered with the excess ligand, preventing the 2-MeIM/Co^{2+} linkage. In the case of the synthesis of ZIF-67 with $Co(NO_3)_2$, a rapid nucleation occurred due to the high instantaneous concentration of Co^{2+} and 2-MeIM ions. Consequently, many small nuclei were formed, shortening the crystal growth stage, resulting in small particles[28,43,47].

The average particle size found for both cases was 280 nm, indicative of nanoparticle synthesis. The particles dried at 25°C exhibited greater uniformity compared to those of ZIF-67 dried at 100°C, which can be attributed to variations in drying and solvent evaporation rates during the synthesis process. The presence of residual solvent within the structure can increase the pore volume and, consequently, the surface area, as evidenced by the BET results. These findings are consistent with the literature, which reports an average particle size ranging from 200 to 400 nm for ZIF-67 synthesized in methanol. For instance, Meshkat et al.[36] obtained an average particle size of 300 nm, and other studies have reported similar findings, with ZIF-67 particles mainly falling within the range of 280 to 400 nm. The particle size and morphology of ZIF-67 are influenced by various factors, such as the solvent used, the concentration of reactants, and the synthesis conditions[36,59-61].

4.2. Membrane Characterization

Figure 4, WAXD curves are presented for PEBAX® MH-1657, ZIF-67, and PEBAX® MH-165/ZIF-67 MMMs. The first image represents MMMs containing ZIF-67, dried at 25 °C, while the second image illustrates MMMs containing ZIF-67 composite membranes, dried at 100 °C. In the neat PEBAX® membrane, the broad peak at $2\theta = 19°$

corresponds to the characteristic amorphous segments of polyethylene oxide (PEO), while the narrow peak at $2\theta = 23.5°$ represents the semicrystalline polyamide (PA) blocks of PEBAX®. The width of the PEO peak is related to the composition of PEBAX®, which consists primarily of PEO (60%). Conversely, the narrower and more intense peak is attributed to the crystallinity of the polyamide component, which constitutes 40% by weight of the copolymer[16,23,38,49,62,63]. The WAXD curves of the MMMs indicate the absence of characteristic peaks associated with ZIF-67, which can be attributed to the low concentration of ZIF in the membrane or to a possible chemical interaction between PEBAX® and ZIF-67 particles. In the case of PEBAX® MH-1657 /5% ZIF-67 MMMs, the presence of crystallographic planes is evident, with higher intensity at approximately $2\theta = 7°$, 10°, 12.5°, 16°, and 18°, corresponding respectively to the characteristic crystallographic planes (011), (002), (112), (013), and (222) of ZIFs[27,46-48,53]. The partial destruction of the crystalline structure during membrane preparation could be inferred, indicating the low stability of the synthesized structure. Another aspect to consider is the low concentrations of ZIF particles in the polymer matrix, which contribute to the absence of characteristic ZIF peaks[27,46].

In order to better understand the stability of ZIF-67 particles produced in Mixed Matrix Membranes (MMMs), the Attenuated Total Reflectance Fourier Transform Infrared Spectroscopy (FTIR-ATR) technique allows for the evaluation of possible chemical interactions between the polymers and ZIF-67. Figure 5 presents the FTIR-ATR spectra obtained for MMMs to analyze the interaction between polymers and ZIF-67. Figure 5 a shows the spectra of MMMs with ZIF-67 dried at 25°C, while Figure 5 b displays the spectra of MMMs with ZIF-67 dried at 100°C. Analyzing the spectrum of pure PEBAX® membrane, characteristic peaks are observed at 1094 cm^{-1}, attributed to C-O-C stretching vibrations within the polyether (PEO) segment, at 1634 cm^{-1}, attributed to stretching vibrations of the carbonyl (C=O) in amides, and at 3298 cm^{-1}, attributed to stretching vibrations of N-H bonds in amides and polyether groups. On the other hand, the peaks observed in the ZIF-67 spectrum were mainly attributed to the 2-methylimidazole ligand[27,36].
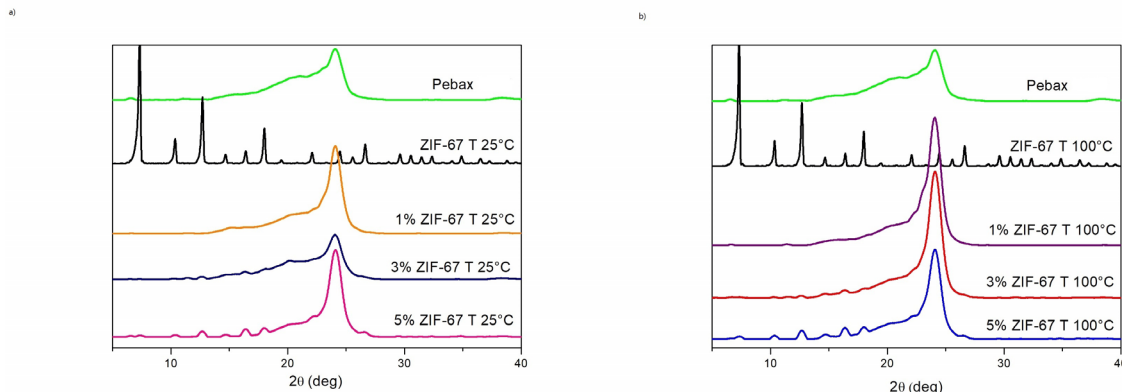

Figure 4. WAXD diffractograms of PEBAX® MH-1657 /ZIF 67 membranes: comparison between the diffractograms of PEBAX® MH-1657 /ZIF 67 membranes. (a) PEBAX® MH-1657, ZIF 67, PEBAX® MH-1657 /ZIF 67 membranes (25 °C) and (b) PEBAX® MH-1657, ZIF 67, PEBAX® MH-1657 /ZIF 67 membranes (100 °C).
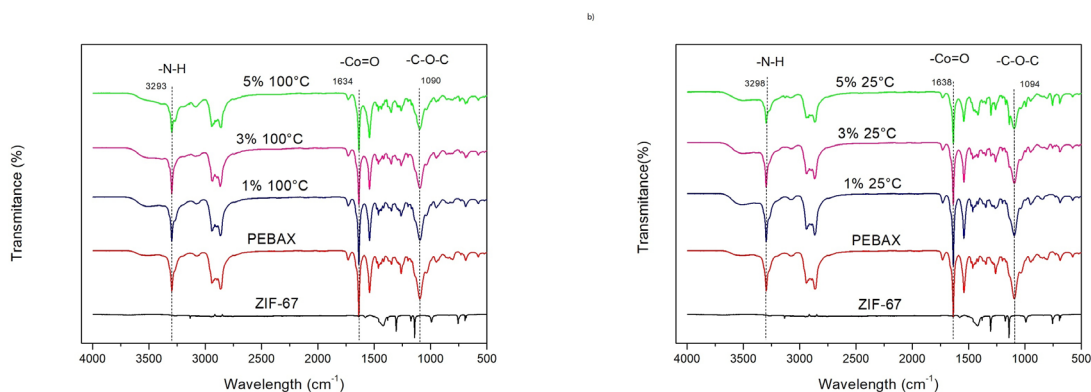
Influence of ZIF-67 Drying Temperatures on the Structure and Properties of PEBAX® MH-1657/ZIF-67 Mixed Matrix Membranes for Enhanced CO$_2$/N$_2$ Separation

7

Figure 5. FTIR-ATR spectra obtained for MMM PEBAX® MH-1657 /ZIF-67.

In the range of 600-1500 cm^{-1}, the peaks were related to the stretching vibration of the imidazole ring, while the peak at 3140 cm^{-1} was attributed to the stretching of the aromatic ring of 2-MeIM. For the spectra of mixed matrix membranes, no new characteristic peaks were observed, indicating that no strong chemical interaction occurs between ZIF-67 and PEBAX®. However, for all MMMs, there was a small shift of the transmittance peak at 3298 cm^{-1} to the left relative PEBAX® MH-1657[27,36,64]. In addition, in membranes containing 5% ZIF-67 (25° C and 100° C), a change in the shape of the same peak, corresponding to the -N-H bond in the secondary amide of PEBAX®, was noted, evidencing a weak interaction between the metal lone pair and nitrogen in the amide. It is concluded that for membranes containing lower amounts of ZIF-67 (1% and 3%), the absence of the discussed characteristic peaks is mainly due to the low concentration of particles in MMMs[36]. However, by increasing the load, as in this case for the 5% membrane, a small interaction between the polymer and the particle occurs due to its instability.

The instability of the synthesized structure in this work, when in contact with an aqueous environment and higher temperatures (~90 °C), can be attributed to the adopted proportional ratio in the synthesis (1:8:1000)[27,36,47,50,53]. The high instantaneous concentration of Co^{2+} ions and 2-MeIM resulted in rapid nucleation of ZIF-67, forming many tiny nuclei, and limiting crystal growth. This led to the formation of small-sized particles with a high surface area of the nanoparticles and exposed Co-N bonds[27,36,47,50].

The absence of sharp peaks associated with ZIF-67 confirms the images obtained by SEM (Figure 6), where the visualization of particles within the matrix is challenging. The provided images correspond to cross-sections of the following samples: PEBAX® MH-1657 /5% ZIF at 25 °C, PEBAX® MH-1657 /1% ZIF at 100 °C, PEBAX® MH-1657 /3% ZIF at 100 °C, and PEBAX® MH-1657 /5% ZIF at 100 °C. In these images, the presence of ZIF-67 agglomerates in the PEBAX® matrix is highlighted by red circles.

DSC curves are displayed in Figure 7. For pure PEBAX® MH-1657, the two endothermic peaks observed correspond to the melting and crystallization temperatures of the polymer components. The Tg of the PEO block was determined to be -50.5 °C, which is consistent with literature[36,45,50]. The Tg, Tm, and crystallinity values of the MMMs are listed in

Table 2. The crystallinity was found to be 18.6% for PEO and 30.9% for PA, while the total crystallinity exhibited by neat PEBAX® membrane was 23.5%. The degree of crystallinity, both for the PEO and PA segments, decreased in all membranes compared to neat PEBAX®, along with the total crystallinity, indicating a transition towards more rubbery states[35,50,65,66]. The crystallinity of the PEO and PA segments is mainly governed by intermolecular bonding (hydrogen bonds), and the addition of particles can disrupt the arrangement of the crystalline phases, leading to reduced crystallinity in the PEBAX® segments. In this case, a chemical interaction between the particles and the matrix suggests a modification in the ordered chain structure of PEBAX®, resulting in increased free volume. This higher presence of free volume also explains the observed variation in Tm (PEO) among the samples[35,50,67].

The decrease in crystallinity increases effective permeation area since crystalline domains are impermeable to gas molecules. Higher permeation area will result in higher permeability which partially explains some of the results obtained in permeation tests. Nevertheless, the increase in permeability is expected with the incorporation of ZIF-67 due to its capacity of adsorbing both CO$_2$ and N$_2$ molecules.

4.3. Gas permeation properties of PEBAX® MH-1657/ZIF-67 membranes

Gas permeation tests were conducted for 3wt% PEBAX® MH-1657 membranes manufactured with a 70/30 ethanol/water mixture at pressures of 3, 5, 10, and 15 bar for N$_2$, CO$_2$, and CH$_4$. Subsequently, permeation tests were carried out for PEBAX® MH-1657 /ZIF-67 mixed matrix membranes only at pressures of 10 and 15 bar for nitrogen and carbon dioxide. The obtained permeability and selectivity values for the respective gas pairs, along with the standard deviation in relation to gas permeation test measurements, are presented in Table 3. for PEBAX® MH-1657 membrane and PEBAX® MH-1657/ZIF-67 mixed matrix membranes.

In general, the permeability of the PEBAX® membrane for N$_2$ remained relatively unchanged with variations in pressure, while there was a notable 2 Barrer increase in CH$_4$ permeability at 10 and 15 bar. Conversely, a substantial
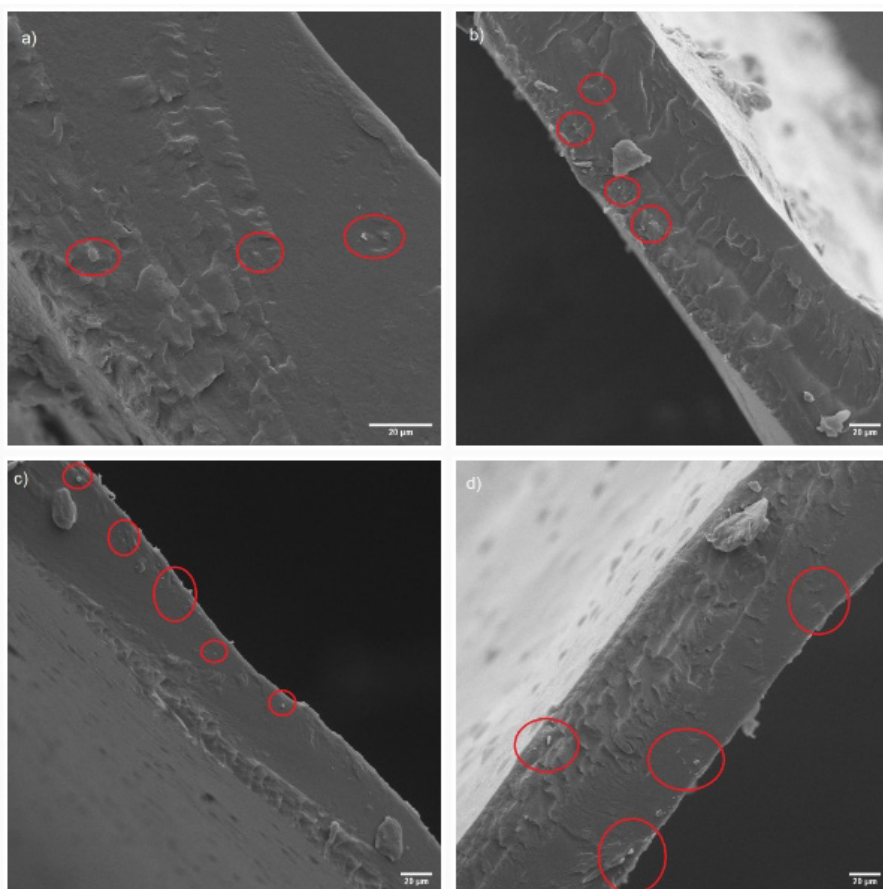
Figure 6. SEM of MMM (Mixed Matrix Membrane) PEBAX® MH-1657 /ZIF-67 at: (a) PEBAX® MH-1657 /5% ZIF T25 °C, (b) PEBAX® MH-1657 /1% ZIF T100, (c) PEBAX® MH-1657 /3% ZIF T100 °C, and (d) PEBAX® MH-1657 /5% ZIF T100 °C.
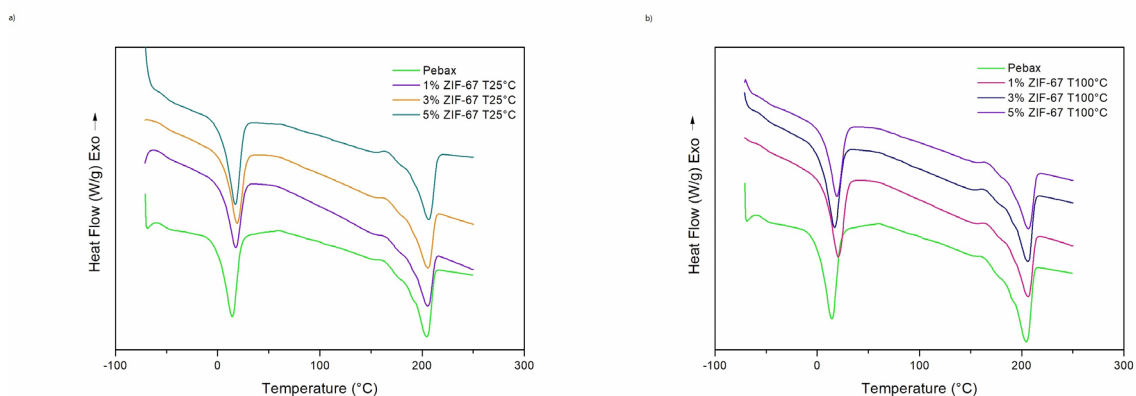

Figure 7. DSC of PEBAX® MH-1657 /ZIF-67 membranes: (a)DSC of PEBAX® MH-1657 /ZIF-67 membranes (25 °C) and (b) PEBAX® MH-1657 /ZIF-67 membranes (100 °C).

increase in CO_2 permeability was evident with escalating pressure. Notably, at 15 bar, the recorded value of 132 Barrer represented a remarkable 79 Barrer increase (150% rise) compared to the initial pressure of 3 bar. This significant surge in gas permeability under increasing pressure can be

ascribed to the enhanced mobility of polymeric chains and the strong interactions between CO_2 and PEO blocks of PEBAX®. The permeability of gases in polymeric membranes is a complex phenomenon influenced by various factors, including pressure, temperature (where higher operating temperatures

Influence of ZIF-67 Drying Temperatures on the Structure and Properties of PEBAX® MH-1657/ZIF-67 Mixed
Matrix Membranes for Enhanced CO$_2$/N$_2$ Separation

9

Table 2. Thermal properties of PEBAX® and PEBAX® MH-1657/ZIF-67 membranes.

Sample	Tg (°C)	T$_m$ (°C) PEO	T$_m$ (°C) PA	X$_c$ (%) PEO	X$_c$ (%) PA	X$_t$ (%)
PEBAX 1657	-50.5	13.5	204.1	18.6	30.9	23.5
1% T.25 °C	-50.3	17.8	205.0	16	23.4	19.2
3% T.25 °C	-50.4	16.1	205.2	18.4	25.4	21.9
5% T.25 °C	-50.2	17.8	206.4	18.5	28.5	23.9
1% T.100 °C	-50.1	14.1	206.1	17.7	24.1	20.5
3% T.100 °C	-49.5	20.1	206.1	14.6	23.8	18.9
5% T.100 °C	-49.7	17.1	206.3	16.6	22.5	19.9

Table 3. Permeability and selectivity values for PEBAX® and PEBAX® MH-1657/ZIF-67 MMMs at different test pressures.

P (bar)	Sample	P N$_2$ (Barrer)	P CH$_4$ (Barrer)	P CO$_2$ (Barrer)	α (CO$_2$/N$_2$)	α (CH$_4$/N$_2$)	α (CO$_2$/CH$_4$)
3	PEBAX 1657	2±0.1	4±0.4	53±0.2	27±0.3	2±0.1	13±1
5	PEBAX 1657	2±0.2	4±0.3	62±1.5	38±2.2	2±0.8	18±0.8
10	PEBAX 1657	2±0.2	6±0.7	114±4	55±0.05	3±1.6	18±0.2
	1% T.25 °C	3±0.21	-	143±4.5	54±2.3	-	-
	3% T.25 °C	3±0.02	-	117±3	44±0.7	-	-
	5% T.25 °C	4±1	-	144±6	40±3	-	-
	1% T.100 °C	3±0.08	-	152±0.2	59±1.9	-	-
	3% T.100 °C	3±0.03	-	126±4	46±3.6	-	-
	5% T.100 °C	3±0.02	-	136±2.4	44±3.2	-	-
15	PEBAX 1657	2±0.2	6±0.57	132±3.5	67±0.03	3±0.1	24±0.3
	1% T.25 °C	2±0.03	-	160±3.8	75±4	-	-
	3% T.25 °C	3±0.01	-	136±3.5	48±1.5	-	-
	5% T.25 °C	4±0.9	-	181.6±5	49±3.5	-	-
	1% T.100 °C	2±0.01	-	164±2.7	74±0.85	-	-
	3% T.100 °C	3±0.4	-	157±0.07	55±3.7	-	-
	5% T.100 °C	3±0.1	-	169±1.3	60±0.6	-	-

1 Barrer = 10^{10} cm^3(STP).cm/cm^2.s.cmHg.

enhance the penetration of gas molecules), and interactions between gas molecules and polymeric chains[30,44,50]. In the specific context of this study, a noteworthy augmentation in gas permeability was observed, primarily attributed to the heightened mobility of polymeric chains and strong interaction of CO$_2$ with PEBAX®. The augmentation in gas pressure in the feed intensified chain mobility, facilitated by a higher concentration of CO$_2$[3,15,22,29,40,44].

The membranes exhibited higher permeability to CO$_2$ compared to other gases (N$_2$ and CH$_4$). Higher CO$_2$ permeability is attributed not only to its kinetic diameter, but also to its solubility in the membrane due to strong dipole-quadrupole interactions between the polar CO$_2$ molecules and the PEO chains of the polymer[45,50,62,67]. Furthermore, the energy distribution of CO$_2$ molecules is lower compared to N$_2$ and CH$_4$, resulting in a more significant interaction between CO$_2$ and the polymeric chains of the membranes, especially in the C=O interactions[33,44]. Regarding selectivity, larger variations were observed for the CO$_2$/N$_2$ pair, followed by CO$_2$/CH$_4$ and CH$_4$/N$_2$. The CO$_2$/N$_2$ pair showed a 150% increase, followed by CO$_2$/CH$_4$ with 85% and CH$_4$/N$_2$ with 50% when comparing the extreme pressure values tested.

For the mixed matrix membranes (MMMs), a slight increase in N$_2$ permeability was observed, but it was not possible to identify a clear relationship between the pressure increase and gas permeability. The presence of fillers disrupts the arrangement of the polymeric chains, increasing the fraction of free volume (FFV) and reducing crystallinity, which influences the gas permeability results. The introduction of ZIF-67 and the resulting structural instability led to an increase in free volume within the matrix, causing the membrane to acquire a rubbery state. This perturbation may be related to the decrease in crystallinity observed in the DSC tests[19,28,36,68,69].

The observed increase in chain mobility with the rise in pressure should theoretically enhance gas permeation. However, the slight increase in N$_2$ permeability despite the increased chain mobility and pressure can be attributed to the restricted polymer chain mobility inherent in the membrane material. This inherent limitation may constrain the extent to which permeability can increase, even with elevated pressure and improved chain mobility. The phenomenon observed aligns with findings in other studies where the permeability of N$_2$ and other gases demonstrated enhancement with increased upstream pressure, but the magnitude of the increase was not as pronounced as that observed for CO$_2$ permeability[70-72]. These observations are influenced by a complex interplay of factors, including the size of the gas molecules and their condensability. As highlighted in the literature, the Langmuir constant increases with a decrease in gas size, and the affinity follows the order CO$_2$ > CH$_4$ > N$_2$.

Consequently, the selective separation of CO_2 from CH_4 in PEBAX® is primarily governed by the higher sorption level of CO_2 in the membrane. This suggests that, despite the increase in chain mobility and pressure, the specific properties of the gases and their interactions with the membrane material can lead to varied permeability responses[73].

The significant increase in CO_2 permeation with the addition of ZIFs is attributed to the electrostatic interactions between the non-coordinated nitrogen atom in the imidazolate ligand and the unsaturated metal sites of the ZIF with CO_2 molecules. The polar nature of CO_2 bonds (C=O) results in their preferential adsorption on the polar walls of the ZIF due to the interaction with the non-coordinated nitrogen atoms present in the polar bonds of the imidazolate. In other words, the nitrogen atoms that are not involved in the coordination bonds of the imidazole ligands and the unsaturated cobalt ions facilitate the dissolution of CO_2 molecules, promoting separation based on CO_2 solubility[43,65,68,69,74].

Another contributing factor is that, in addition to the strong dissolution of carbon dioxide in the PEBAX® MH-1657/ZIF-67 membrane, CO_2 molecules not only perform diffusional jumps from one free volume to another, but the pores present in ZIF-67 also act as additional pathways for the gas. Therefore, the substantially enhanced CO_2 permeability in PEBAX® MH-1657/ZIF-67 MMMs is a consequence of the simultaneous increase in gas diffusivity and solubility. Membranes containing 1% ZIF-67 exhibited the highest CO_2 permeability and selectivity at 10 bar pressure, with selectivities of 54 and 59 for ZIF-67 MMMs at 25 °C and 100 °C, respectively. The same behavior is observed with the pressure increase to 15 bar. The membranes with 1% ZIF at 25 °C and 100 °C exhibited a CO_2/N_2 selectivity of 75, an increase of approximately 28% compared to the same concentration and pressure of 10 bar. For better visualization, the obtained values are shown in Figure 8 in the form of a graph, illustrating the effect of pressure on CO_2 permeability and ideal selectivity of CO_2/N_2 and CO_2/CH_4 for PEBAX® membranes (a), and for MMMs, the obtained values and concentration graphs of ZIF-67 as a function of CO_2 permeability and ideal selectivity of CO_2/N_2 at pressures of (b) 10 bar and (c) 15 bar.

The performance of the investigated membranes was evaluated using Robeson's upper bound, which is widely recognized as a reference standard in the membrane scientific community. The upper bound sets a metric that new membranes should surpass, with the ideal selectivity/permeability being directed towards the upper right corner of Robeson's plot[11-13]. Although the trade-off and upper bound are not decisive in membrane separation processes, they serve as practical tools for comparing the properties of different materials. In the case of pure PEBAX® MH-1657 membranes (Figure 9a), the CO_2/CH_4 selectivity relative to the CO_2 permeability remains below the limit proposed by Robeson in 1991 at all tested pressures. As the feed pressure increases, there is a noticeable increase in the selectivity/permeability ratio of the membranes. At 10 bar, the results indicate a similar selectivity range to that obtained in the membranes tested at 5 bar. It is important to note that at these two pressures, although the CO_2 permeability has almost doubled with the increase in pressure, the methane permeability also follows
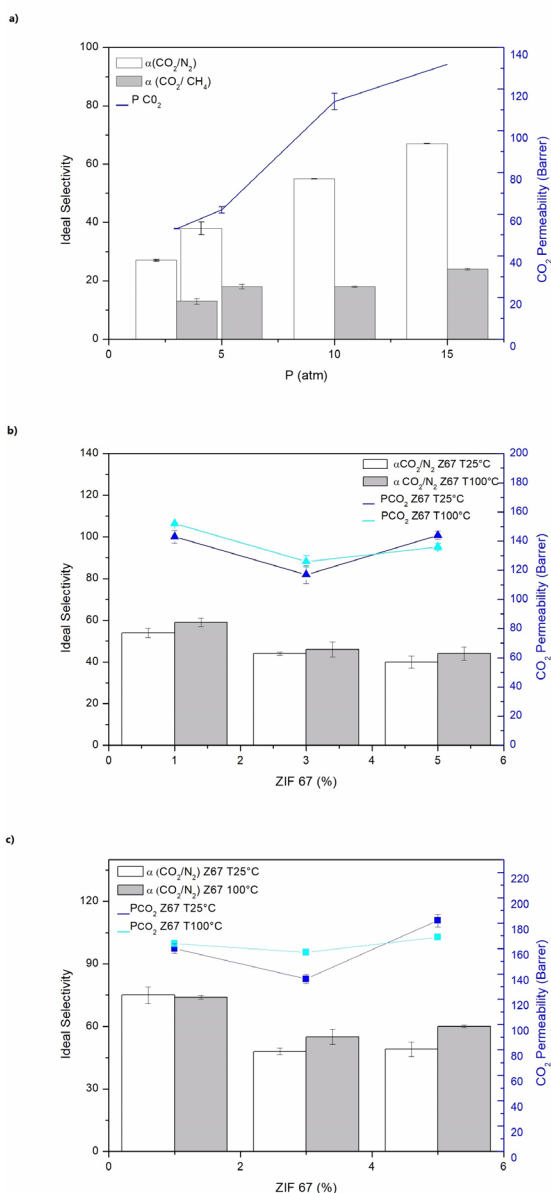
Figure 8. CO2 permeability and ideal selectivity for: (a) PEBAX® MH-1657 under different pressures. (b) Effect of filler loading on PEBAX® MH-1657/ZIF-67 membranes at 35 °C and 10 atm (c) Effect of filler loading on PEBAX® MH-1657 /ZIF-67 membranes at 35 °C and 15 atm.

the same trend. At a pressure of 15 bar, the membrane is positioned above and to the right of the membrane tested at 10 bar. This suggests that at higher pressures, the selectivity between the CO_2/CH_4 gas pair improves, as well as the CO_2 permeability, suggesting better CH_4 retention. Therefore, membranes located higher and to the right on the graph are considered to have better performance[11,12,15,37].

As observed from the CO_2/N_2 upper bound (Figure 9b), the PEBAX® MH-1657/ZIF-67 MMMs exhibited inferior performance compared to pure PEBAX®. For tests conducted at a pressure of 15 bar, the membranes composed only of PEBAX® MH-1657 performed better than the PEBAX® MH-
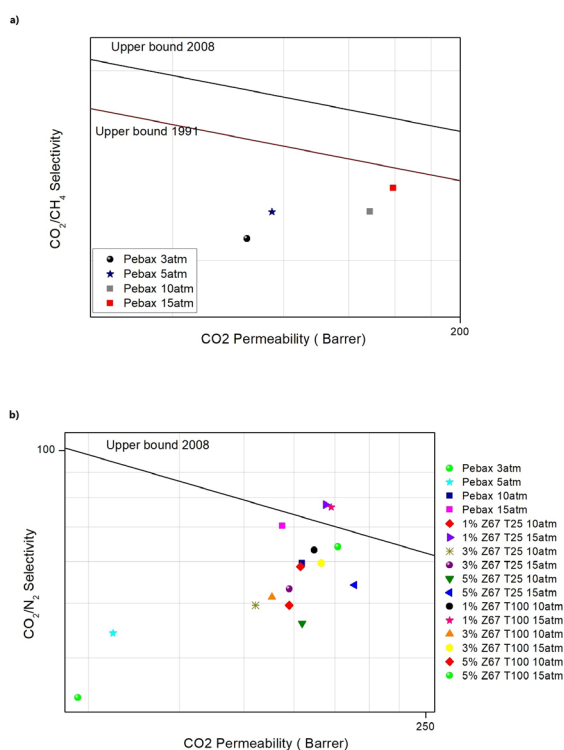
Influence of ZIF-67 Drying Temperatures on the Structure and Properties of PEBAX® MH-1657/ZIF-67 Mixed
Matrix Membranes for Enhanced CO₂/N₂ Separation

11

Table 4. Values derived from the literature, presenting gas permeation data for PEBAX® MH-1657/ZIFS MMMs with different loadings.

Sample	ZIFcontent (% wt)	P (bar)	P N_2 (Barre)	P CH4 (Barre)	PCO_2 (Barrer)	α (CO_2/N_2)	α (CO_2/CH_4)	Ref.
PEBAX®-5%-GO/core shell ZIF	5	1	2.8	9.9	173.2	61.9	11.6	Liu et al.[45]
PEBAX® -10%-GO/*core shell* ZIF	10	1	2.1	6.1	95.1	46.2	8.4	Liu et al.[45]
PEBAX® / ZIF-94	10	3	-	-	137	36	-	Hasan et al.[75]
PEBAX®/ZIF-67	3	11	2.1	5.7	154.3	72.5	-	Meshkat[36]
PEBAX® /ZIF-67	5	11	2	6.5	162	81	-	Meshkat[36]
PEBAX® /ZIF-8	3	11	2.7	6.3	125	46.6	20	Meshkat[36]
PEBAX® /ZIF-8	5	11	2.8	7	130	47.6	18.6	Meshkat[36]
PEBAX® /ZIF-67-L	10	2	-	-	91.6	51.8	-	Zhao et al.[50]
PEBAX® / ZIF-67 25°C	1	15	2.1	-	160	75	-	This work
PEBAX® / ZIF-67 100°C	1	15	2.2	-	164	74	-	This work
PEBAX® / ZIF-67 100°C	1	10	2.6	-	152	60	-	This work

1657/ZIF-67 MMMs with 3% and 5% loading under both drying conditions. This result is likely due to the incorporation of ZIF-67 into the membrane and its effective destabilization of the PEBAX® segments. Although CO_2 permeability remained relatively constant with applied pressure, N_2 permeability increased, and the ideal CO_2/N_2 selectivity was moderately reduced[19,22,33,50,74]. The only compositions that showed improvements compared to pure PEBAX® MH-1657 at 15 bar were the 1% ZIF-67 concentrations at 15 bar. These two samples not only outperformed pure PEBAX® but also exceeded the Robeson upper bound of 2008.

The influence of ZIF-67 concentration on gas permeability and selectivity could be explained by interactions between ZIF-67 and PEBAX® MH-1657. These interactions could reduce local molecular mobility increasing the selectivity of the mixed matrix membranes. Based on these interface effects, the higher selectivity of PEBAX® MH-1657/ ZIF-67 MMMs with 1wt% of ZIF-67 could be the result of better dispersion of ZIF-67 particles. It is well known that the dispersion of small particles is challenging due to their higher surface energies and tendency to agglomerate[36,43,48,50]. Nanocomposites are usually produced by incorporating low contents of nanofillers because of the difficult in dispersion. Because ZIF-67 have the non-coordinated nitrogen atom in the imidazolate ligand and the unsaturated metal sites that interact with CO_2, it is likely that they will tend to agglomerate. With the increase in ZIF-67 concentration, the presence of agglomerates reduces the interactions between ZIF-67 and PEBAX® and the selectivity decreases[36,46-48,50].

In Table 4, we present permeability and selectivity results taken from the literature for the purpose of comparison with the values obtained in the MMMs PEBAX® MH-1657/ ZIF so far. We highlight the findings of Meshkat et al.[36], who examined membranes of PEBAX® MH-1657 and ZIF-67 containing 3% and 5% of filler. They observed a selectivity of 72.5 and 81, respectively, at a pressure of 11 bar. However, for ZIF-8, the values were 46.6 and 47.6. This disparity arises from the effectiveness of ZIF-67 in facilitating the diffusion of CO_2, while ZIF-8 contributes to enhancing the solubility of CO_2. Meshkat et al.[36] explain that the stronger electrostatic interactions between the Zn metal center of ZIF-8 and CO_2 molecules limit the rapid diffusion of CO_2[43].

Figure 9. Performance of the Pebax® and PEBAX® MH-1657/ ZIF-67 membranes on Robeson plots for: (a) CO2/CH4 (PEBAX® MH-1657) and (b) CO_2/N_2.

It is also relevant to consider the amount of added filler. Filler concentrations above 10 wt% for ZIF-67 can compromise the selectivity of the MMM due to particle agglomeration and the formation of intergranular defects. Salahshoori et al.[44], in their research, found that increasing the addition of fillers from 5 wt% to 20 wt% does not alter the performance of the PEBAX® MH-1657/ZIF-67 membranes. In contrast, Zhao et al.[50] concluded that the ideal performance is achieved with 10 wt% by weight, resulting in a CO_2 permeability of 91.4 Barrer and a CO_2/N_2 selectivity of 51.7. The addition of ZIF-67 fillers at this concentration showed significant improvements, increasing the CO_2 permeability by 74.1% and the CO_2/N_2 selectivity by 23.6% in pure gas measurements.

The values highlighted in the table were obtained under different pressure conditions, and as mentioned earlier, pressure has a significant effect on gas separation. In general, the low concentration of 1 wt% of ZIF-67 added provided better results among the produced MMMs. When compared with other values in the table, both membranes containing PEBAX® MH-1657/1% ZIF-67 resulted in higher CO_2 permeability and selectivity for the CO_2/N_2 gas pair. The superior results obtained by Meshkat et al.[36] were with a higher concentration of 5% ZIF-67. However, in this study we report a challenge in particle dispersion for loadings above 1%, especially with results obtained for membranes containing 5%. This challenge is justifiable due to the inefficiency of dispersion during membrane production. Additionally, the smaller average particle size of 280 nm is another factor that implies greater particle agglomeration.

5. Conclusions

ZIF-67 particles, synthesized with a molar ratio of 1:8:1000 of cobalt nitrate hexahydrate, 2-methylimidazole, and methanol, exhibited an average size of 280 nm and a high surface area. The drying temperature influenced the particle surface area, with crystals dried at 25°C showing a higher surface area attributed to larger pores generated by residual solvent presence. Analysis of PEBAX® MH-1657/ ZIF-67 MMMs with compositions of 1%, 3%, and 5% by weight, regardless of drying temperature (25 °C or 100 °C), revealed the absence or weak presence of characteristic ZIF-67 peaks, confirmed by FTIR-ATR analysis. In membranes with 5 wt% ZIF-67, a change in the shape of the -N-H bond peak in PEBAX® indicated a weak interaction between the metal lone pair and nitrogen in the amide. The absence of characteristic peaks in MMMs with lower ZIF-67 amounts (1 wt% and 3 wt%) was attributed to low particle concentration, while the 5 wt% membrane exhibited a weak polymer-particle interaction due to instability. This instability was justified by the 1:8:1000 synthesis ratio, leading to rapid ZIF-67 nucleation, hindering growth, exposing Co-N bonds, and resulting in high nanoparticle surface area. The matrix-particle interaction reduced the MMMs' crystallinity compared to the pure PEBAX® membrane.

Gas permeation in PEBAX® MH-1657/ZIF-67 MMMs was influenced by matrix-particle interaction, with CO_2 permeation surpassing that of N_2 and CH_4 due to smaller kinetic diameter, higher condensability, polarization capacity, and weaker interaction with the ether (PEO) group of PEBAX® and ZIF-67 particles. The reduced crystallinity further enhanced gas molecule passage, achieving superior results to Robeson's 2008 upper bound for CO_2/N_2 in PEBAX® MH-1657/ZIF-67 MMMs containing 1% load.

6. Acknowledgments

7. References

1. Baker RW, Lokhandwala K. Natural gas processing with membranes: an overview. Ind Eng Chem Res. 2008;47(7):2109-21. http://dx.doi.org/10.1021/ie071083w.

2. Favvas EP, Katsaros FK, Papageorgiou SK, Sapalidis AA, Mitropoulos AC. A review of the latest development of polyimide based membranes for CO_2 separations. React Funct Polym. 2017;120:104-30. http://dx.doi.org/10.1016/j.reactfunctpolym.2017.09.002.

3. Yang L, Zhang S, Wu H, Ye C, Liang X, Wang S, et al. Porous organosilicon nanotubes in pebax-based mixed-matrix membranes for biogas purification. J Membr Sci. 2019;573:301-8. http://dx.doi.org/10.1016/j.memsci.2018.12.018.

4. Lin H, Freeman BD. Materials selection guidelines for membranes that remove CO_2 from gas mixtures. J Mol Struct. 2005;739(1-3):57-74. http://dx.doi.org/10.1016/j.molstruc.2004.07.045.

5. Scholes CA, Stevens GW, Kentish SE. Membrane gas separation applications in natural gas processing. Fuel. 2012;96:15-28. http://dx.doi.org/10.1016/j.fuel.2011.12.074.

6. Zhao D, Ren J, Wang Y, Qiu Y, Li H, Hua K, et al. High CO_2 separation performance of Pebax®/CNTs/GTA mixed matrix membranes. J Membr Sci. 2017;521:104-13. http://dx.doi.org/10.1016/j.memsci.2016.08.061.

7. Abhisha VS, Swapna VP, Stephen R. Modern trends and applications of gas transport through various polymers. In: Thomas S, Wilson R, Kumar A, Soney S, George C, editors. Transport properties of polymeric membranes. USA: Elsevier; 2018. p. 363-89.. http://dx.doi.org/10.1016/B978-0-12-809884-4.00018-5.

8. Eiras D, Labreche Y, Pessan LA. Ultem®/ZIF-8 mixed matrix membranes for gas separation: transport and physical properties. Mater Res. 2016;19(1):220-8. http://dx.doi.org/10.1590/1980-5373-MR-2015-0621.

9. Hasegawa M, Tokunaga R, Hashimoto K, Ishii J. Crosslinkable polyimides obtained from a reactive diamine and the effect of crosslinking on the thermal properties. React Funct Polym. 2019;139:181-8. http://dx.doi.org/10.1016/j.reactfunctpolym.2019.04.005.

10. Recio R, Lozano ÁE, Prádanos P, Marcos Á, Tejerina F, Hernández A. Effect of fractional free volume andTg on gas separation through membranes made with different glassy polymers. J Appl Polym Sci. 2008;107(2):1039-46. http://dx.doi.org/10.1002/app.26542.

11. Robeson LM, Liu Q, Freeman BD, Paul DR. Comparison of transport properties of rubbery and glassy polymers and the relevance to the upper bound relationship. J Membr Sci. 2015;476:421-31. http://dx.doi.org/10.1016/j.memsci.2014.11.058.

12. Robeson LM, Smith ZP, Freeman BD, Paul DR. Contributions of diffusion and solubility selectivity to the upper bound analysis for glassy gas separation membranes. J Membr Sci. 2014;453:71-83. http://dx.doi.org/10.1016/j.memsci.2013.10.066.

13. Park HB, Kamcev J, Robeson LM, Elimelech M, Freeman BD. Maximizing the right stuff: the trade-off between membrane permeability and selectivity. Science. 1979;2017(356):1138-48.

14. Matteucci S, Yampolskii Y, Freeman BD, Pinnau I. Transport of gases and vapors in glassy and rubbery polymers. In: Yuri Y, Ingo P, Benny F, editors. Materials science of membranes for gas and vapor separation. Chichester: Wiley; 2006. p. 1-47.. http://dx.doi.org/10.1002/047002903X.ch1.

15. Kim NU, Park BJ, Guiver MD, Kim JH. Use of non-selective, high-molecular-weight poly(ethylene oxide) membrane for CO_2 separation by incorporation of comb copolymer. J Membr Sci. 2020;605:118092. http://dx.doi.org/10.1016/j.memsci.2020.118092.

16. Nobakht D, Abedini R. Improved gas separation performance of Pebax®1657 membrane modified by poly-alcoholic compounds. J Environ Chem Eng. 2022;10(3):107568. http://dx.doi.org/10.1016/j.jece.2022.107568.

Influence of ZIF-67 Drying Temperatures on the Structure and Properties of PEBAX® MH-1657/ZIF-67 Mixed
Matrix Membranes for Enhanced CO₂/N₂ Separation

13

17. Klopffer MH, Flaconnèche B. Transport properties of gases in polymers: bibliographic review. Oil Gas Sci Technol. 2001;56(3):223-44. http://dx.doi.org/10.2516/ogst:2001021.

18. Kanehashi S, Kusakabe A, Sato S, Nagai K. Analysis of permeability; solubility and diffusivity of carbon dioxide; oxygen; and nitrogen in crystalline and liquid crystalline polymers. J Membr Sci. 2010;365(1-2):40-51. http://dx.doi.org/10.1016/j.memsci.2010.08.035.

19. Martínez-Izquierdo L, Malankowska M, Sánchez-Laínez J, Téllez C, Coronas J. Poly(ether- block -amide) copolymer membrane for CO₂/N₂ separation: the influence of the casting solution concentration on its morphology, thermal properties and gas separation performance. R Soc Open Sci. 2019;6(9):190866. http://dx.doi.org/10.1098/rsos.190866.

20. Nagel C, Günther-Schade K, Fritsch D, Strunskus T, Faupel F. Free volume and transport properties in highly selective polymer membranes. Macromolecules. 2002;35(6):2071-7. http://dx.doi.org/10.1021/ma011028d.

21. Ricci E, Minelli M, De Angelis MG. Modelling sorption and transport of gases in polymeric membranes across different scales: a review. Membranes. 2022;12(9):857. http://dx.doi.org/10.3390/membranes12090857.

22. Reijerkerk SR, Wessling M, Nijmeijer K. Pushing the limits of block copolymer membranes for CO₂ separation. J Membr Sci. 2011;378(1-2):479-84. http://dx.doi.org/10.1016/j.memsci.2011.05.039.

23. Ahmad S, Lian S, Tan Y, Li R, Zhao Q, Song C, et al. Solvent influence on the textural properties and CO₂/N₂ separation performance of novel Pebax-1657/attapulgite mixed matrix membranes. J Environ Chem Eng. 2021;9(5):105806. http://dx.doi.org/10.1016/j.jece.2021.105806.

24. Fodor C, Kali G, Thomann R, Thomann Y, Iván B, Mülhaupt R. Nanophasic morphologies as a function of the composition and molecular weight of the macromolecular cross-linker in poly(N-vinylimidazole)-l-poly(tetrahydrofuran) amphiphilic conetworks: bicontinuous domain structure in broad composition ranges. RSC Advances. 2017;7(12):6827-34. http://dx.doi.org/10.1039/C6RA25356C.

25. Alhamami M, Doan H, Cheng C. A review on breathing behaviors of metal-organic-frameworks (MOFs) for gas adsorption. Materials. 2014;7(4):3198-250. http://dx.doi.org/10.3390/ma7043198.

26. Zhang J, Tan Y, Song WJ. Zeolitic imidazolate frameworks for use in electrochemical and optical chemical sensing and biosensing: a review. Mikrochim Acta. 2020;187(4):234. http://dx.doi.org/10.1007/s00604-020-4173-3.

27. Feng S, Bu M, Pang J, Fan W, Fan L, Zhao H, et al. Hydrothermal stable ZIF-67 nanosheets via morphology regulation strategy to construct mixed-matrix membrane for gas separation. J Membr Sci. 2020;593:117404. http://dx.doi.org/10.1016/j.memsci.2019.117404.

28. Jomekian A, Bazooyar B, Behbahani RM, Mohammadi T, Kargari A. Ionic liquid-modified Pebax® 1657 membrane filled by ZIF-8 particles for separation of CO₂ from CH4, N2 and H2. J Membr Sci. 2017;524:652-62. http://dx.doi.org/10.1016/j.memsci.2016.11.065.

29. Jeong S, Sohn H, Kang SW. Highly permeable PEBAX-1657 membranes to have long-term stability for facilitated olefin transport. Chem Eng J. 2018;333:276-9. http://dx.doi.org/10.1016/j.cej.2017.09.125.

30. Azizi N, Mohammadi T, Behbahani RM. Synthesis of a PEBAX-1074/ZnO nanocomposite membrane with improved CO₂ separation performance. Journal of Energy Chemistry. 2017;26(3):454-65. http://dx.doi.org/10.1016/j.jechem.2016.11.018.

31. Meshkat S, Kaliaguine S, Rodrigue D. Mixed matrix membranes based on amine and non-amine MIL-53(Al) in Pebax® MH-1657 for CO₂ separation. Separ Purif Tech. 2018;200:177-90. http://dx.doi.org/10.1016/j.seppur.2018.02.038.

32. Clarizia G, Bernardo P. A review of the recent progress in the development of nanocomposites based on poly(ether-block-amide) copolymers as membranes for CO₂ separation. Polymers. 2021;14(1):10. http://dx.doi.org/10.3390/polym14010010.

33. Zhao H, Ding X, Yang P, Li L, Li X, Zhang Y. A novel multi-armed and star-like poly(ethylene oxide) membrane for CO₂ separation. J Membr Sci. 2015;489:258-63. http://dx.doi.org/10.1016/j.memsci.2015.04.028.

34. Casado-Coterillo C, Fernández-Barquín A, Valencia S, Irabien Á. Estimating CO₂/N₂ permselectivity through Si/Al = 5 Small-Pore Zeolites/PTMSP mixed matrix membranes: influence of temperature and topology. Membranes. 2018;8(2):32. http://dx.doi.org/10.3390/membranes8020032.

35. Carreon M, Dahe G, Feng J, Venna SR. Mixed matrix membranes for gas separation applications. In: Carreon MA, editor. Membranes for gas separations. Singapura: World Scientific; 2017. p. 1-57. http://dx.doi.org/10.1142/9789813207714_0001.

36. Meshkat S, Kaliaguine S, Rodrigue D. Comparison between ZIF-67 and ZIF-8 in Pebax® MH-1657 mixed matrix membranes for CO₂ separation. Separ Purif Tech. 2020;235:116150. http://dx.doi.org/10.1016/j.seppur.2019.116150.

37. Hamley IW. Ordering in thin films of block copolymers: fundamentals to potential applications. Prog Polym Sci. 2009;34(11):1161-210. http://dx.doi.org/10.1016/j.progpolymsci.2009.06.003.

38. Chung T, Jiang LY, Li Y, Kulprathipanja S. Mixed matrix membranes (MMMs) comprising organic polymers with dispersed inorganic fillers for gas separation. Prog Polym Sci. 2007;32(4):483-507. http://dx.doi.org/10.1016/j.progpolymsci.2007.01.008.

39. Xiang L, Pan Y, Zeng G, Jiang J, Chen J, Wang C. Preparation of poly(ether-block-amide)/attapulgite mixed matrix membranes for CO₂/N₂ separation. J Membr Sci. 2016;500:66-75. http://dx.doi.org/10.1016/j.memsci.2015.11.017.

40. Wang L, Li Y, Li S, Ji P, Jiang C. Preparation of composite poly(ether block amide) membrane for CO₂ capture. J Energy Chem. 2014;23(6):717-25. http://dx.doi.org/10.1016/S2095-4956(14)60204-7.

41. Chernikova V, Shekhah O, Eddaoudi M. Advanced fabrication method for the preparation of MOF thin films: liquid-phase epitaxy approach meets spin coating method. ACS Appl Mater Interfaces. 2016;8(31):20459-64. http://dx.doi.org/10.1021/acsami.6b04701.

42. Nafisi V, Hägg M-B. Development of dual layer of ZIF-8/PEBAX-2533 mixed matrix membrane for CO₂ capture. J Membr Sci. 2014;459:244-55. http://dx.doi.org/10.1016/j.memsci.2014.02.002.

43. Wu X, Liu W, Wu H, Zong X, Yang L, Wu Y, et al. Nanoporous ZIF-67 embedded polymers of intrinsic microporosity membranes with enhanced gas separation performance. J Membr Sci. 2018;548:309-18. http://dx.doi.org/10.1016/j.memsci.2017.11.038.

44. Salahshoori I, Babapoor A, Seyfaee A. Elevated performance of the neat, hybrid and composite membranes by the addition of nanoparticles (ZIF-67): a molecular dynamics study. Polym Bull. 2022;79(6):3595-630. http://dx.doi.org/10.1007/s00289-021-03673-2.

45. Liu N, Cheng J, Hou W, Yang X, Zhou J. Pebax-based mixed matrix membranes loaded with graphene oxide/core shell ZIF-8@ZIF-67 nanocomposites improved CO₂ permeability and selectivity. J Appl Polym Sci. 2021;138(23):50553. http://dx.doi.org/10.1002/app.50553.

46. Du X-D, Wang C-C, Liu J-G, Zhao X-D, Zhong J, Li Y-X, et al. Extensive and selective adsorption of ZIF-67 towards organic dyes: performance and mechanism. J Colloid Interface Sci. 2017;506:437-41. http://dx.doi.org/10.1016/j.jcis.2017.07.073.

47. Guo X, Xing T, Lou Y, Chen J. Controlling ZIF-67 crystals formation through various cobalt sources in aqueous solution. J Solid State Chem. 2016;235:107-12. http://dx.doi.org/10.1016/j.jssc.2015.12.021.

48. Tran NT, Kim J, Othman MR. Microporous ZIF-8 and ZIF-67 membranes grown on mesoporous alumina substrate for selective propylene transport. Separ Purif Tech. 2020;233:116026. http://dx.doi.org/10.1016/j.seppur.2019.116026.

49. Surya Murali R, Ismail AF, Rahman MA, Sridhar S. Mixed matrix membranes of Pebax-1657 loaded with 4A zeolite for gaseous separations. Separ Purif Tech. 2014;129:1-8. http://dx.doi.org/10.1016/j.seppur.2014.03.017.

50. Zhao Q, Lian S, Li R, Yang Y, Zang G, Song C. Fabricating Leaf-like hierarchical ZIF-67 as Intra-Mixed matrix membrane microarchitecture for efficient intensification of CO_2 separation. Separ Purif Tech. 2023;305:122460. http://dx.doi.org/10.1016/j.seppur.2022.122460.

51. Song Q, Nataraj SK, Roussenova MV, Tan JC, Hughes DJ, Li W, et al. Zeolitic imidazolate framework (ZIF-8) based polymer nanocomposite membranes for gas separation. Energy Environ Sci. 2012;5(8):8359-69. http://dx.doi.org/10.1039/c2ee21996d.

52. Zhang H, Liu D, Yao Y, Zhang B, Lin YS. Stability of ZIF-8 membranes and crystalline powders in water at room temperature. J Membr Sci. 2015;485:103-11. http://dx.doi.org/10.1016/j.memsci.2015.03.023.

53. Nazir MA, Khan NA, Cheng C, Shah SSA, Najam T, Arshad M, et al. Surface induced growth of ZIF-67 at Co-layered double hydroxide: removal of methylene blue and methyl orange from water. Appl Clay Sci. 2020;190:105564. http://dx.doi.org/10.1016/j.clay.2020.105564.

54. Wang M, Liu J, Guo C, Gao X, Gong C, Wang Y, et al. Metal-organic frameworks (ZIF-67) as efficient cocatalysts for photocatalytic reduction of CO_2: the role of the morphology effect. J Mater Chem A Mater Energy Sustain. 2018;6(11):4768-75. http://dx.doi.org/10.1039/C8TA00154E.

55. Zhang Y, Tong Y, Li X, Guo S, Zhang H, Chen X, et al. Pebax mixed-matrix membrane with highly dispersed ZIF-8@CNTs to enhance CO_2/N_2 separation. ACS Omega. 2021;6(29):18566-75. http://dx.doi.org/10.1021/acsomega.1c00493.

56. Wu C, Xie D, Mei Y, Xiu Z, Poduska KM, Li D, et al. Unveiling the thermolysis natures of ZIF-8 and ZIF-67 by employing in situ structural characterization studies. Phys Chem Chem Phys. 2019;21(32):17571-7. http://dx.doi.org/10.1039/C9CP02582K.

57. Maleh MS, Raisi A. Heteroepitaxial growth of ZIF-67 nanoparticles on the ZIF-L(Zn) nanosheets for fabrication of Pebax mixed matrix membranes with highly efficient CO_2 separation. Chemosphere. 2023;344:140249. http://dx.doi.org/10.1016/j.chemosphere.2023.140249.

58. Saeed S, Bashir R, Rehman SU, Nazir MT, ALOthman ZA, Muteb Aljuwayid A, et al. Synthesis and characterization of ZIF-67 mixed matrix nanobiocatalysis for CO_2 adsorption performance. Front Bioeng Biotechnol. 2022;10:891549. http://dx.doi.org/10.3389/fbioe.2022.891549.

59. Davoodi M, Davar F, Rezayat MR, Jafari MT, Bazarganipour M, Shalan AE. Synthesis and characterization of a new ZIF-67@MgAl2O4 nanocomposite and its adsorption behaviour. RSC Advances. 2021;11(22):13245-55. http://dx.doi.org/10.1039/D1RA01056E.

60. Saliba D, Ammar M, Rammal M, Al-Ghoul M, Hmadeh M. Crystal growth of ZIF-8, ZIF-67, and their mixed-metal derivatives. J Am Chem Soc. 2018;140(5):1812-23. http://dx.doi.org/10.1021/jacs.7b11589.

61. Duan C, Yu Y, Hu H. Recent progress on synthesis of ZIF-67-based materials and their application to heterogeneous catalysis. Green Energy Environ. 2022;7(1):3-15. http://dx.doi.org/10.1016/j.gee.2020.12.023.

62. Li M, Zhang X, Zeng S, Bai L, Gao H, Deng J, et al. Pebax-based composite membranes with high gas transport properties enhanced by ionic liquids for CO_2 separation. RSC Advances. 2017;7(11):6422-31. http://dx.doi.org/10.1039/C6RA27221E.

63. Nobakht D, Abedini R. A new ternary Pebax ® 1657 / maltitol / ZIF-8 mixed matrix membrane for efficient CO_2 separation. Process Saf Environ Prot. 2023;170:709-19. http://dx.doi.org/10.1016/j.psep.2022.12.058.

64. Taheri P, Maleh MS, Raisi A. Cross-linking of poly (ether-block-amide) by poly (ethylene glycol) diacrylate to prepare plasticizing-resistant CO_2-selective membranes. J Environ Chem Eng. 2021;9(5):105877. http://dx.doi.org/10.1016/j.jece.2021.105877.

65. Thompson JA, Vaughn JT, Brunelli NA, Koros WJ, Jones CW, Nair S. Mixed-linker zeolitic imidazolate framework mixed-matrix membranes for aggressive CO_2 separation from natural gas. Microporous Mesoporous Mater. 2014;192:43-51. http://dx.doi.org/10.1016/j.micromeso.2013.06.036.

66. Chen XY, Tien-Binh N, Kaliaguine S, Rodrigue D. Polyimide membranes for gas separation: synthesis, processing and properties. New York: Nova Science Publishers; 2016.

67. Xu L, Xiang L, Wang C, Yu J, Zhang L, Pan Y. Enhanced permeation performance of polyether-polyamide block copolymer membranes through incorporating ZIF-8 nanocrystals. Chin J Chem Eng. 2017;25(7):882-91. http://dx.doi.org/10.1016/j.cjche.2016.11.007.

68. Li Y, Li X, Wu H, Xin Q, Wang S, Liu Y, et al. Anionic surfactant-doped Pebax membrane with optimal free volume characteristics for efficient CO_2 separation. J Membr Sci. 2015;493:460-9. http://dx.doi.org/10.1016/j.memsci.2015.06.046.

69. Sutrisna PD, Hou J, Li H, Zhang Y, Chen V. Improved operational stability of Pebax-based gas separation membranes with ZIF-8: a comparative study of flat sheet and composite hollow fibre membranes. J Membr Sci. 2017;524:266-79. http://dx.doi.org/10.1016/j.memsci.2016.11.048.

70. Kadirkhan F, Goh PS, Ismail AF, Wan Mustapa WNF, Halim MHM, Soh WK, et al. Recent advances of polymeric membranes in tackling plasticization and aging for practical industrial CO_2/CH_4 applications: a review. Membranes. 2022;12(1):71. http://dx.doi.org/10.3390/membranes12010071.

71. Houben M, Kloos J, van Essen M, Nijmeijer K, Borneman Z. Systematic investigation of methods to suppress membrane plasticization during CO_2 permeation at supercritical conditions. J Membr Sci. 2022;647:120292. http://dx.doi.org/10.1016/j.memsci.2022.120292.

72. Zhang M, Deng L, Xiang D, Cao B, Hosseini SS, Li P. Approaches to suppress CO_2-induced plasticization of polyimide membranes in gas separation applications. Processes. 2019;7(1):51. http://dx.doi.org/10.3390/pr7010051.

73. Vaughn JT, Koros WJ. Analysis of feed stream acid gas concentration effects on the transport properties and separation performance of polymeric membranes for natural gas sweetening: a comparison between a glassy and rubbery polymer. J Membr Sci. 2014;465:107-16. http://dx.doi.org/10.1016/j.memsci.2014.03.029.

74. Shekhah O, Chernikova V, Belmabkhout Y, Eddaoudi M. Metal-organic framework membranes: from fabrication to gas separation. Crystals. 2018;8(11):412. http://dx.doi.org/10.3390/cryst8110412.

75. Hasan M, Paseta L, Malankowska M, Téllez C, Coronas J. Synthesis of ZIF-94 from recycled mother liquors: study of the influence of its loading on postcombustion CO_2 capture with pebax based mixed matrix membranes. Adv Sustainable Syst. 2022;6(1):2100317. http://dx.doi.org/10.1002/adsu.202100317.